

Dust destruction in bubbles driven by multiple supernovae explosions

Evgenii O. Vasiliev¹, Biman B. Nath²

¹Lebedev Physical Institute, Russian Academy of Sciences, 53 Leninsky Avenue, Moscow 119991, Russia;

²Department of Physical Sciences, Indian Institute of Science Education and Research (IISER) Mohali, Knowledge City, Sector 81, Sahibzada Ajit Singh Nagar, Punjab 140306, India;

Accepted XXX. Received YYY; in original form ZZZ

ABSTRACT

Dust lifetime derived from an isolated supernova (SN) evolution in the interstellar medium is known to be an order of magnitude shorter than the time needed to replenish dust mass by its production in various Galactic sources. We show, with the help of 3-D numerical hydrodynamical simulations, that destruction of dust in the case of multiple SNe in a star cluster is markedly different from that in an isolated SN. We find that the mass of dust destroyed in the bubble does not grow for a considerable time, while SNe continue to explode. This regime is attained at saturation timescale, which is proportional to SNe rate in cluster. We show that the mass of dust destroyed in bubble per SN decreases for higher SN rate. Thus, the destruction efficiency – defined as the ratio of the total mass of dust destroyed by clustered SNe to that destroyed by the same number of isolated SNe – in bubbles evolved in a homogeneous medium drops for massive clusters, e.g. around clusters with $M_* \gtrsim 4 \times 10^4 M_\odot$ it is less 0.4%. For lower mass clusters, the efficiency is proportional to the average time delay between SNe. We found that each cluster with $M_* \lesssim 4 \times 10^4 M_\odot$ destroys the same mass of dust as a single isolated SN. In a clumpy medium with lognormal distribution of density fluctuations having dispersion $\sigma \sim 2.2$ and a spatial Kolmogorov power-law spectrum, the efficiency increases by a factor of ~ 1.5 in bubbles formed around clusters with $M_* \sim 4 \times 10^4 M_\odot$ and up to 4 times around $M_* \sim 8 \times 10^5 M_\odot$. We argue that the interstellar dust swept up by multiple SNe almost completely survives in the shells of bubbles around such massive clusters. Therefore, the destruction of the interstellar dust is controlled by SNe in low-mass clusters. We point out that the interstellar dust lifetime for a given SN rate is at least a factor ~ 10 longer as compared to the estimates derived from an isolated SN.

Key words: Interstellar dust; Interstellar dust processes; Supernova remnants

1 INTRODUCTION

Interstellar dust is thought to be destroyed by the inertial and thermal sputtering in hot gas (Barlow 1978; Draine & Salpeter 1979b,a; McKee 1989; Jones et al. 1994; Nath et al. 2008; Slavin et al. 2015; Priestley et al. 2022, and references therein). In cold gas, surviving dust can be shattered in grain-grain collisions at higher densities, replenishing the population of smaller grains (Borkowski & Dwek 1995; Jones et al. 1996; Slavin et al. 2004; Guillet et al. 2009; Bocchio et al. 2016; Kirchschlager et al. 2019). During further evolution, these grains can be entrained by strong shocks and may again be found in hot environment. The typical rate of shocks in the Galactic interstellar medium implies a characteristic dust lifetime that ranges between $3 \times 10^8 - 10^9$ yr (McKee 1989; Jones et al. 1994; Jones & Tielens 1994; Slavin et al. 2015). Such short time scale, compared to the dust production time (McKee 1989; Draine 2009), raises an important question regarding the dust mass budget in the ISM (see for recent discussion in Mattsson 2021; Kirchschlager et al. 2022; Péroux et al. 2023), which is commonly referred to as the ‘dust budget crisis’ (Michałowski et al. 2010; Dunne et al. 2011; Rowlands et al. 2014).

The problem can be briefly explained as follows. Dust is efficiently sputtered by shocks with speeds as high as $\gtrsim 200$ km/s. Such speeds are typical for SN expansion at adiabatic phase in the diffuse interstellar gas. During this period, the kinetic energy of SN shell is of

the order of the SN energy: $Mv_s^2 \sim E_{SN}$. This results in an estimate of the swept-up interstellar material by a single isolated SN of about $10^3 M_\odot$ (McKee 1989; Draine 2009). From this, the destroyed dust mass can be estimated to be of order of $10 M_\odot$ per SN, if the gas-to-dust mass is ~ 100 . Using this result, the authors (McKee 1989) obtained the dust lifetime for the Galactic SN rate as $\tau \sim 4 \times 10^8$ yr. This timescale is shorter by than a factor around 20 the dust replenishment time from AGB stars and SNe (Draine 2009). The mismatch makes it difficult to explain the existence of dust in the interstellar medium.

This estimate is, however, valid only for isolated SN explosions. In the case of multiple SNe, which is more common than isolated SN, because stellar SN progenitors are typically located in OB-associations (e.g., Krumholz et al. 2019), the situation can be different. In the bubble produced by multiple SNe explosions, the efficiency of dust destruction can be markedly different because subsequent explosions occur inside hot rarefied gas, so that when the shock fronts finally interact with a dense shell, the shocks would have lost much of their energy. A similar scenario occurs when a SN explodes in a pre-existing HII region, where the shell is formed by an ionization front (Martínez-González et al. 2019). The speed of shocks of the subsequent SNe falls below 200 km/s after interacting with the dense shell. Therefore, one can expect that the damped shocks lose their ability to destroy dust in the shell, at least due to sputtering.

Here we consider in detail for the first time the destruction of dust in the shells driven by multi-SNe. The paper is organized as follows. Section 2 describes the model details. Section 3 presents the evolution of the swept-up interstellar dust in bubbles driven by multiple-SNe explosions in stellar clusters. In Section 4 we summarize our results and possible consequences.

2 MODEL DESCRIPTION

Let us consider a star cluster of mass M_* . The number of SN in it is $N_{SN} \sim M_*/150 M_\odot$ for a Salpeter initial mass function (IMF) for stellar masses in the range of $0.1 - 40 M_\odot$. SNe progenitors are thought to have masses in range $8 - 40 M_\odot$. The duration of SNe explosions spans the lifetime of the least massive star of $8M_\odot$ $t_{lf,max} \sim 24$ Myr ($t_{lf} \sim M^{-1.6}$) (Iben 2013). The average time between SN explosions in a cluster is, therefore, $\Delta t \sim 24$ Myr/ N_{SN} . For example, in a cluster of $M_* \sim 4 \times 10^4 M_\odot$, the number of SNe is $N_{SN} \sim 250$ and the average time delay between explosions is $\Delta t \sim 10^5$ yr.

The mass function of stellar clusters is $dN/dM \sim M^{-\alpha}$, where $\alpha = 1.25 - 2.25$, $M_{min} \sim 10^3 M_\odot$, $M_{max} \sim 3 \times 10^7 M_\odot$ (Krumholz et al. 2019). The estimate above shows that the higher the cluster mass M_* , the higher the SN rate, or, equivalently, the shorter the time delay between explosions: $\Delta t \sim 3600$ Myr/ M_* . Our models with different Δt describe clusters of varying masses, since $M_* \propto \Delta t^{-1}$.

We carry out 3D hydrodynamic simulations of the ISM under the action of multiple clustered SNe explosions. SNe are distributed uniformly and randomly inside a region with a fixed cluster radius $r_c = 10$ pc. Note that this value is close to the half-mass radius of stellar clusters r_h with mass $\sim 10^7 M_\odot$ (the $r_h - M_*$ relation increases slightly more slowly than $r_h \sim M_*^{1/3}$ (see Figure 9 in Krumholz et al. 2019)). We have assumed one SN per $\Delta t = 100, 50, 30, 10$ and 5 kyr, which correspond to clusters of masses $M_* \sim 4 \times 10^4, 8 \times 10^4, 1.2 \times 10^5, 4 \times 10^5$ and $8 \times 10^5 M_\odot$, the last one being the upper limit of stellar cluster mass in the Milky Way (see, e.g. Krumholz et al. 2019). We inject the mass and energy of a SN in a region of radius $r_0 = 3$ pc, assuming commonly used values $M_{inj} = 30 M_\odot$ and $E = 10^{51}$ erg. The energy is injected in thermal form, although the results are not sensitive to the form of injected energy (Sharma et al. 2014).

We consider primarily single-sized interstellar dust with size equal to $a_0 = 0.1 \mu\text{m}$. During the evolution, dust grains are destroyed and their sizes decrease depending on physical conditions in ambient gas; the minimum size is set to $0.01 \mu\text{m}$.

The gas distribution in the ambient (background) medium is set to be homogeneous with density $n_b = 1 \text{ cm}^{-3}$ as a fiducial value, the temperature in all models is 10^4 K. We study the case of a clumpy medium in a later section 3.1. The metallicity of the background gas is equal to solar value $[\text{Z}/\text{H}] = 0$. We assume a dust-to-gas (DtG) mass ratio equal to $\zeta_b = 0.01$.

Simulations are run with tabulated non-equilibrium cooling rates for a gas that cools isochorically from 10^8 down to 10 K (Vasiliev 2011, 2013). The heating rate is assumed to be constant, with a value chosen such as to stabilize the radiative cooling of the ambient gas at $T = 10^4$ K.

We use our gas-dynamic code (Vasiliev et al. 2015, 2017) based on the unsplit total variation diminishing (TVD) approach that provides high-resolution capturing of shocks and prevents unphysical oscillations, and the Monotonic Upstream-Centered Scheme for Conservation Laws (MUSCL)-Hancock scheme with the Haarten-Lax-van Leer-Contact (HLLC) method (see e.g. Toro 2009) as approximate

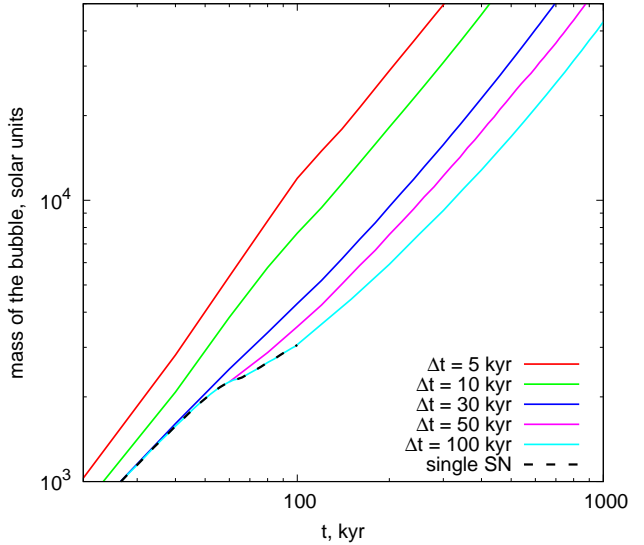


Figure 1. Mass of the bubble driven by multiple SNe explosions in a cluster. The color lines depict the evolution for different rates, of one SN per $\Delta t = 100, 50, 30, 10$ and 5 kyr.

Riemann solver. This code has successfully passed the whole set of tests proposed in (Klingenberg et al. 2007). In order to follow the dynamics of dust particles we have implemented the method (see description and tests in Appendix A of Vasiliev & Shchekinov 2024) similar to that proposed in the papers (Youdin & Johansen 2007; Mignone et al. 2019; Moseley et al. 2023). The backward reaction of dust on to gas due to momentum transfer, work done by the drag force and the frictional heating from dust particles are also accounted for in order to ensure both dynamical and thermal self-consistency. We take into account the destruction of dust particles by both thermal (in a hot gas) and kinetic (due to a relative motion between gas and grains) sputtering (Draine & Salpeter 1979a).

The mass of dust in a medium is distributed between many dust ‘superparticles’. Each ‘superparticle’ is supposed to represent an ensemble of numerous physical grains of a single size. To follow the dust transport in a medium we set at least one ‘superparticle’ per computational cell. Each ‘superparticle’ contains the total mass of the ensemble of single-sized dust particles in it. So the total dust mass in a cell is a sum of masses of ‘superparticles’ inside a cell (see for more details Vasiliev & Shchekinov 2024).

The cell size equal to 1 pc is adopted for the runs with ambient gas number density $n = 1 \text{ cm}^{-3}$. This is sufficient for resolving the thermal (cooling) length estimated as $\lambda_t \sim 5 n^{-1} T_6$ pc. The numerical grid consists of 256^3 cells. This results in the total number of interstellar dust ‘superparticles’ in the domain being $256^3 \sim 16$ millions.

3 DYNAMICS

Fig. 1 presents the total mass of gas within the bubble (including injected and swept up mass), created by multiple SNe exploded in a cluster with different SN rate, as a function of time. The dashed line (which is run for only 100 kyr) is shown as a benchmark. The total bubble mass asymptotically grows as $t^{9/5}$, which is expected from the self-similar evolution of wind bubbles ($r \propto t^{3/5}$). The bubble driven by SNe of rate $(100 \text{ kyr})^{-1}$, for example, attains this

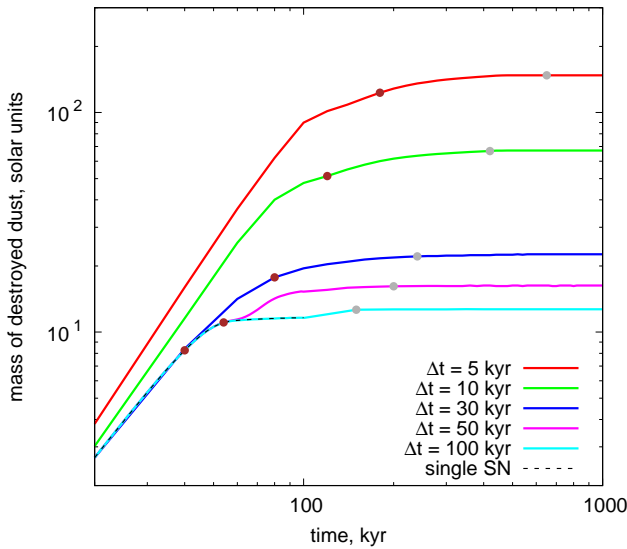


Figure 2. Mass of dust destroyed in the bubble for the models presented in Fig. 1. The brown points correspond to the saturation time according to eq. 1, whereas the grey points refer to the onset of radiative phase of bubbles ($v \sim 100 \text{ km s}^{-1}$).

slope after $t \sim 400 - 500$ kyr. More massive clusters attain the wind regime at earlier epochs.

The mass of interstellar dust destroyed behind the front evolves as in Fig. 2. For low SN rate it follows the dependence for a single SN. For higher rates the destroyed dust mass increases linearly. Later, the rate of increase slows down and eventually saturates approximately as $\Delta t^{-1/2}$. Therefore, the flat part of the curves in Figure 2 represents the saturation regime when the total mass of destroyed dust does not increase while the SNe continue to explode. The saturation is linked to the fact that the shock speed falls below $v_0 \sim 200 \text{ km s}^{-1}$, corresponding to post-shock temperature of $\sim 10^6 \text{ K}$. The saturation in dust destruction occurs at a time scale, given by,

$$t_{sat} \sim v_0^{-5/2} \left(\frac{\rho \Delta t}{E} \right)^{-1/2}. \quad (1)$$

The brown points in Fig. 2 correspond to this epoch, with $v_0 = 200 \text{ km s}^{-1}$. The curves show that saturation is reached at longer time scales for higher SN rate, i.e. in bubbles around more massive stellar clusters. Incidentally, this also happens to be close to the epoch when a multiple SNe bubble of radius $R \sim (E t^3 / \Delta t \rho)^{1/5}$ becomes radiative when the velocity is of the order of $v_0 \sim 100 \text{ km s}^{-1}$ because at this point the post-shock temperature corresponds to a peak in the cooling curve.

In young adiabatic SN remnants, the dust is efficiently sputtered in the shell behind the shock front. Later, when the shell becomes radiative, the dust destruction rate decreases, and the incoming dust gets to compensate for earlier losses of dust mass. This fact manifests itself in a low value of the dust-to-gas ratio ρ_d / ρ_g in the shell, when the shock velocity $v_s \gtrsim 200 \text{ km/s}$, and which increases when the gas behind the shock cools down to $T_s \lesssim 10^6 \text{ K}$. In bubbles driven by multiple SNe, one has the same scenario. (see details in Appendix and in Fig A1).

As one can see, in the bubble formed by multiple SNe with rate $(\Delta t)^{-1} \sim (100 \text{ kyr})^{-1}$ the mass of destroyed dust reaches $\sim 13 M_\odot$ after explosions of three SNe at $t \sim 200$ kyr and does not grow at later time. Note that a single isolated SN destroys roughly the same mass of dust: $M_1 \sim 13 M_\odot$. Using the established prescription (McKee

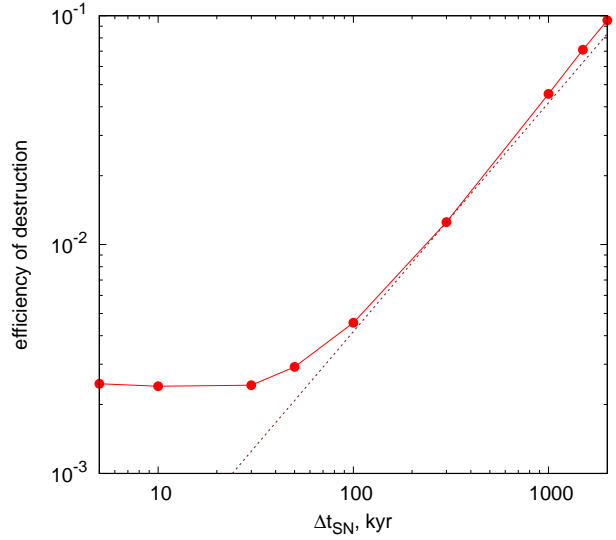


Figure 3. The dust destruction efficiency, i.e. the ratio of the the total mass of dust destroyed by SNe in cluster to the value of dust destroyed by the same number of isolated SNe. The dash line follows $\Delta t / t_{lf,max}$, where $t_{lf,max} \sim 24 \text{ Myr}$.

1989; Draine 2009) one expects that these three SNe would destroy $\sim 3M_1 \sim 39 M_\odot$ of dust and this value, therefore, increases as $N_{SN} M_1$. However, as one can conclude from Fig. 2, the mass of destroyed dust saturates at some level and subsequent SNe do not destroy dust. For example, during the evolution of a cluster with $M_* \sim 4 \times 10^4 M_\odot$ ($\Delta t = 100 \text{ kyr}$) the total number of SNe is $N_{SN} \sim 250$. If each of these SNe had exploded in an isolated manner, they would have destroyed in total $N_{SN} M_1 = 3 \times 10^3 M_\odot$. However, Fig. 2 shows that this mass is about $\sim 15 M_\odot$, which is about 200 times lower than the expected value.

Clusters with masses in the range $M_* \sim (4 - 12) \times 10^4 M_\odot$ with a time delay $\Delta t \sim 30 - 100 \text{ kyr}$ and the mean number of SNe of $N_{SN} \sim 500$ per cluster would have destroyed in total $\sim 6.5 \times 10^4 M_\odot$ if they had exploded in an isolated manner. However, according to our calculations such a cluster destroys only $\sim 20 M_\odot$ (it lies between cyan and blue lines in Fig. 2).

SNe exploding in clusters of $M_* \lesssim 4 \times 10^4 M_\odot$ with a time delay $\Delta t \gtrsim 100 \text{ kyr}$ destroy the same mass of dust as that by a single SN: $M_1 \sim 13 M_\odot$. This remains valid unless the time delay between subsequent SNe is shorter than the fadeaway time (when the SN expansion velocity has slowed to the sound speed in the preshock medium c_s), which is $t_f \sim 1 \text{ Myr}$ for a single SN evolved in gas with $n \sim 1 \text{ cm}^{-3}$ and $c_s \sim 10 \text{ km/s}$ for $T \sim 10^4 \text{ K}$ (Draine 2011). After $t_f \gtrsim 1 \text{ Myr}$ the SN cavity is filled by the gas from the SN shell. A shock from the next SN propagates again into the gas already processed by the previous SN shocks. During this process the interstellar dust swept-up in the shell can also partially enter the warm ($T \sim 10^4 - 10^5 \text{ K}$) and low-density ($n \sim 0.1 \text{ cm}^{-3}$) cavity. In our numerical calculations the mass of such dust reaches around $\lesssim 1 - 2 M_\odot$ for the delay between SNe longer than $\sim 1 \text{ Myr}$. This dust is destroyed by subsequent SNe. Thus, in such low-mass clusters the mass of the destroyed dust is close to that by a single SN, i.e. it differs slightly from M_1 .

At longer time delay $\Delta t \sim 3 \text{ Myr}$ in very low-mass clusters of $M_* \sim 10^3 M_\odot$, the cavity can be filled not only by the gas of the shell, but also presumably by the interstellar gas containing unprocessed dust.

This matter can be carried on into the cavity by interstellar turbulent flows. In our calculations we do not include such flows. However, one can estimate that for (super)sonic turbulence the cavity can be filled by the unprocessed interstellar material within a few million years. This issue will be studied in detail elsewhere. Therefore, a next SN explodes in the medium with properties (density, dust fraction) close to those being in the medium before the first SN has exploded. Thus, each SN in such low-mass clusters destroys the same dust mass as that by a set of SNe explode in isolation, it can be estimated as $N_{SN} M_1 \sim (M_*/150 M_\odot) M_1$.

The destruction efficiency can be determined as the ratio of the total mass of dust destroyed by SNe in cluster to the value of dust destroyed by the same number of isolated SNe $M_1 \times N_{SN}$. This efficiency is shown in Fig. 3 as a function of Δt . We find that for large Δt , or equivalently, small number of SNe, the efficiency of dust destruction increases, while for large number of SNe in clusters more massive than $M_* \gtrsim 10^5 M_\odot$ with a time delay $\Delta t \lesssim 30$ kyr, it reaches an asymptotic value of ~ 0.0025 .

Another asymptotics is reached for intermediate and low-mass clusters of $M_* \lesssim 4 \times 10^4 M_\odot$ with a time delay $\Delta t \gtrsim 100$ kyr (Fig. 3). All SNe in a single such cluster are able to destroy the same mass of dust as an isolated SN. The destruction efficiency follows $\sim \Delta t/t_{lf,max}$, where $t_{lf,max} \sim 24$ Myr is the lifetime of the least massive star of $8M_\odot$, which can be a SN progenitor. A small difference of our numerical models for $\Delta t \gtrsim 1$ Myr from the simple linear function depicted by dash line comes from the destruction of the dust entered to the cavity during fadeaway phase.

At very low-mass clusters of $M_* \sim 10^3 M_\odot$ with a time delay a few times longer than the fadeaway time, i.e. $\Delta t \sim 3$ Myr, the cavity is assumed to be filled by the unprocessed interstellar material owing to the (super)sonic interstellar turbulence. Thus, we expect that each SN in such low-mass clusters destroys the dust mass estimated as $(M_*/150 M_\odot) M_1$.

Thus, in the bubbles formed around massive clusters of $M_* \gtrsim 4 \times 10^4 M_\odot$ or with average time delay between SNe explosions $\Delta t \lesssim 100$ kyr, the efficiency of dust destruction is equal about $\epsilon_d \sim 0.004$. For lower mass clusters of $M_* \lesssim 4 \times 10^4 M_\odot$ the efficiency is proportional to $\epsilon_d \sim \Delta t/t_{lf,max}$. Finally, for very low-mass clusters of $M_* \sim 10^3 M_\odot$ it is expected to be close to unity.

The number of SNe in clusters $M_* \gtrsim 4 \times 10^4 M_\odot$, i.e. with delay $\Delta t \lesssim 100$ kyr, is about 60% of the total number of SNe, since

$$f_{SN,h} \sim \frac{\int_{M_*}^{M_{max}} M^{-\alpha+1} dM}{\int_{M_{min}}^{M_{max}} M^{-\alpha+1} dM} \approx 0.6, \quad (2)$$

assuming the limits M_{min} , M_{max} to be equal to $10^3 M_\odot$ and $3 \times 10^7 M_\odot$, respectively, and the index $\alpha \sim 2$ (Krumholz et al. 2019).

Summarizing, the interstellar dust destroyed in the bubbles driven by multiple SNe in stellar clusters is $\sim \int \epsilon_d(M_*) N_{SN}(M_*) M_1 dM_*$, where ϵ_d is the destruction efficiency in a cluster with mass of M_* . In high mass clusters of $M_* \gtrsim 4 \times 10^4 M_\odot$ with $\Delta t \lesssim 100$ kyr the mass of the destroyed dust can be estimated as $\sim \epsilon_{d,h} N_{SN,h} M_1$, where $\epsilon_{d,h} \sim 0.0025$ (see Fig. 3), $N_{SN,h}$ is the total number of SNe in the high-mass clusters of $M_* \gtrsim 4 \times 10^4 M_\odot$, $N_{SN,h} \simeq f_{SN,h} N_{SN,tot}$, $N_{SN,tot}$ is the total number of SNe in all clusters, $f_{SN,h} \sim 0.6$ from eq. 2. Each cluster with Δt from ~ 100 kyr to a few Myr destroys the dust mass equal to M_1 . Thus, the mass of the destroyed dust is $\sim \epsilon_{d,m} N_{SN,m} M_1$, where $\epsilon_{d,m} \sim \Delta t/24$ Myr (see Fig. 3), $N_{SN,m} \simeq f_{SN,m} N_{SN,tot}$, $f_{SN,m} \sim 0.3$ from eq. 2 using the appropriate limits. SNe in clusters $M_* \sim (1-2) \times 10^3 M_\odot$ is assumed to destroy the dust mass with $\epsilon_{d,l} \sim 1$, the fraction number of SNe in such clusters is $f_{SN,l} \sim 0.1$.

Thus, the total mass of the interstellar dust destroyed in bubbles around clusters can be estimated as $(\epsilon_{d,h} f_{SN,h} + \epsilon_{d,m} f_{SN,m} + \epsilon_{d,l} f_{SN,l}) N_{SN,tot} M_1$. Note that the mass destroyed by the same number of SNe exploding in isolation is $\sim N_{SN,tot} M_1$. Thus, the ratio between the two is the efficiency of dust destruction, $\epsilon = \epsilon_{d,h} f_{SN,h} + \epsilon_{d,m} f_{SN,m} + \epsilon_{d,l} f_{SN,l}$. The first term is about 2.5×10^{-4} , as one see below this value is negligible compared to the others. The second term increases linearly with Δt . We can estimate the second term for an average mass cluster of $M_* \sim 9 \times 10^3 M_\odot$ with $\Delta t \sim 400$ kyr (the average value corresponds to the half of the fraction number of SNe in clusters of $M_* \sim 2 \times 10^3 - 4 \times 10^4 M_\odot$), $\epsilon_{d,m} \sim 0.016$ (see also Fig. 3), which gives the second term is $\sim 4.5 \times 10^{-3} \ll 0.1$. The third term for clusters $M_* \sim (1-2) \times 10^3 M_\odot$ gives the major contribution, which is ~ 0.1 for $\epsilon_{d,l} \sim 1$. In case of lower efficiency value, the ratio ϵ decreases. Therefore, the total ratio is ~ 0.1 for the cluster mass function with the index $\alpha \sim 2$ (Krumholz et al. 2019). Hence, the dust lifetime in the interstellar medium becomes longer by a factor ~ 10 compared to the value derived from the isolated SN evolution (McKee 1989). The dust budget crisis mentioned in the Introduction can thus be, if not totally resolved, mitigated to a large extent by taking into account the fact that most SNe occur in clusters and the effect of multiple SNe for dust destruction is different from that of an isolated SN.

Note that we have used equal intervals between SNe. The interval between subsequent explosions corresponds in average to the lifetime of massive stars within $8 - 40 M_\odot$: $t \sim M^{-1.57}$ (Iben 2013). In massive clusters the number of stars being SN progenitors is large enough to produce frequent SNe explosions with more or less constant rate within several million years after the most massive star has exploded. At the same time in low-mass clusters there are a few massive stars, i.e. the initial mass function (IMF) has large gaps in the range $8 - 40 M_\odot$. Thus, the intervals between subsequent SNe explosions can be long enough and vary significantly from one stellar cluster to another. This manifests in the mass of dust destruction being dependent on the IMF of the cluster.

Although the efficiency of dust destruction is low in bubbles around massive clusters, their number is quite small compared to low-mass ones. Therefore, the destruction of the interstellar dust is controlled by SNe in low-mass clusters and the total budget of interstellar dust depends on the lowest mass M_{min} of stellar cluster, where at least one star massive as $M > 8M_\odot$ can be formed.

The results mentioned so far pertains to an ambient density $n = 1 \text{ cm}^{-3}$. Next, we vary the ambient density in our simulation runs. Fig. 4 presents the total mass of dust destroyed in the bubble driven by SNe per $\Delta t = 10$ and 5 kyr as a function of the ambient gas density n . The curve shows that the destroyed dust mass decreases approximately as $M_d \propto n^{-1/3}$. In a denser environment, the wind shock slows down faster, and consequently, sputtering ceases at an earlier epoch, leading to less efficiency of dust destruction. Since the shock speed scales as $v \propto n^{-1/5} t^{-2/5}$, roughly, the epoch when sputtering is considerably diminished, i.e. when the wind bubble shock speed reaches a value $v_0 \sim 200 \text{ km/s}$, approximately scales as $t_{sp} \propto n^{-1/2}$. The mass of destroyed dust scales roughly as $\propto n R(t_{sp})^3$, or equivalently, as $\propto n^{-1/2}$ (accounting the bubble radius reaches $R(t_{sp}) \propto (t_{sp}^3/n)^{1/5}$). This is indeed the slope in Fig. 4 for $n \lesssim 10 \text{ cm}^{-3}$.

3.1 Sequential SN explosions in a clumpy environment

In the foregoing sections, we considered dust destruction in the bubble that evolve in a uniform medium. In a clumpy medium the bubble

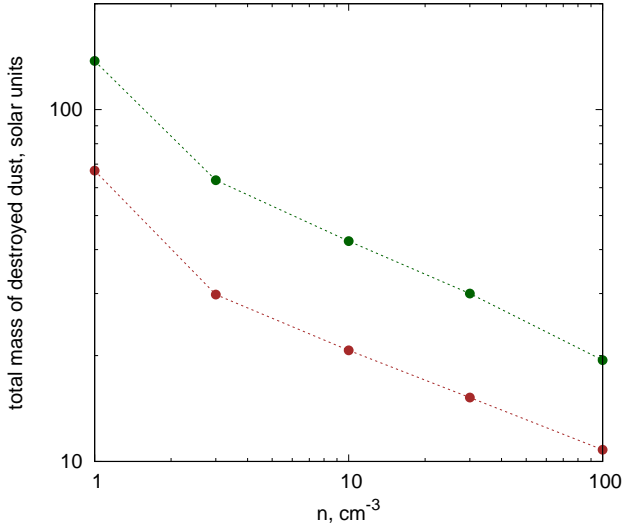


Figure 4. Total mass of dust destroyed in the bubble driven by SNe with the rate one per $\Delta t = 10$ and 5 kyr (green and brown lines, respectively) in the medium with gas number density n .

dynamics differs because the shock penetrates through a medium with finite-sized obstacles that are randomly distributed along its path. When a shock wave encounters a dense clump it drives a converging shock wave inwards with velocity $v_{in} \sim \chi^{-1/2} v_{out}$ (Bychkov & Pikelner 1975), where $\chi = \rho_{in}/\rho_{out}$ is the density contrast (*i.e.*, the ratio of the clump ρ_{in} to the interclump ρ_{out} density), and $v_{out} = v_s$ is the shock velocity. The parts of the shock that lie outside the projected clump area, flow around the clump and penetrate into the low-density interclump gas in the form of ‘long tongues’ (e.g. Poludnenko et al. 2002; Korolev et al. 2015; Slavin et al. 2017; Wang et al. 2018). As a result, the shock wave between clumps remains adiabatic on a longer time scale, and propagates through the diffuse low-density gas with a relatively higher velocity. In the self-consistent gas-dust dynamics the authors (Dedikov & Vasiliev 2025b) have shown that the dust mass fraction destroyed in the bubble from a single SN in a clumpy medium is less than that in a homogeneous medium. Similar conclusion has been obtained for a SN remnant in a turbulent medium using the post-processing for dust dynamics (Scheffler et al. 2025). This is because the dust confined in dense and partly-destroyed clumps does not suffer sputtering because the converging shock weakens as $v_s \propto \rho^{-1/2}$ (Bychkov & Pikelner 1975). It is important to stress that each clump around the SN experiences the shock impact only once. In other words, once engulfed, the clump remains safe from being shocked again.

On the contrary, the clumps in bubbles driven by multiple SNe suffer impacts from shocks episodically as long as the SNe explode. Each such encounter perturbs the medium enveloping the clump and strip it through the action of various hydrodynamic instabilities (Kelvin-Helmholtz, Rayleigh-Taylor and Richtmyer-Meshkov). This results in continuously repeated shock encounters, affecting the dust confined in clumps, and it increases the mass fraction of the destroyed dust. Despite this fact, the inner parts of clumps can survive continuous shock impacts due to radiative losses and strong density contrast. In such conditions, a substantial fraction of confined dust is protected against sputtering.

To study the dust destruction in multiple-SNe driven bubbles, we construct a clumpy gas density field by making use of the module

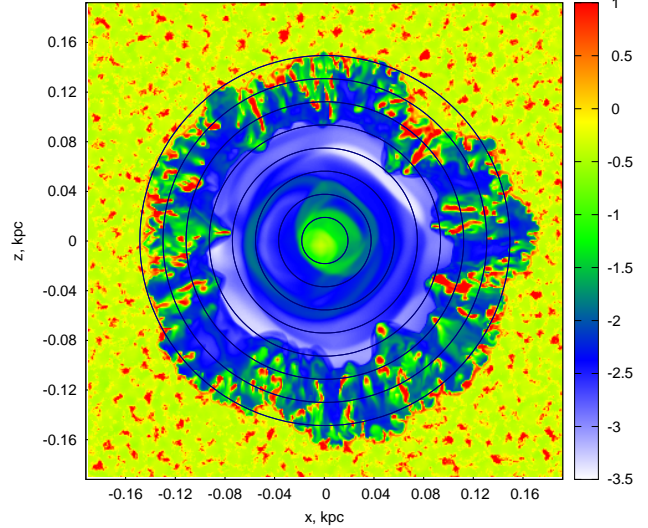


Figure 5. The $y = 0$ plane slice of the gas density distribution in the bubble from clustered SNe in a clumpy medium with the average density $\langle \rho \rangle = 1 m_H \text{ g cm}^{-3}$ at the age $t = 800$ kyr. Black circles roughly outline the forward shock at times $t = 20, 60, 100, 200, 300, 440, 580$ and 800 kyr. Engulfed clumps being episodically impacted by upcoming shocks are seen to be deformed and compressed. At the same time, they are accelerated but because of compression they remain deep behind the forward shock.

pyFC¹ (Lewis & Austin 2002) which generates lognormal ‘fractal cubes’. Within this model the gas density fluctuations in the ambient medium have a lognormal distribution and a Kolmogorov power-law spectrum with spatial index $\beta = 5/3$ and maximum size of inhomogeneities equal to 16 pc. The density field is characterised by the mean $\langle \rho \rangle$ and the standard deviation σ for logarithmic value. We consider a density field with $\sigma = 2.2$, which corresponds to the contrast for 2σ fluctuations exceeding a factor of $\gtrsim 80$ related to the mean value $\langle \rho \rangle = 1 \text{ cm}^{-3}$. We assume pressure equilibrium at the initial state, *i.e.*, $\rho T = \text{const}$, with zero gas and dust velocities. Thus, the gas temperature values differ by a factor of $\gtrsim 80$ between dense cloudlets and the intercloud medium.

The gas behind the SNe shock front in a cloudy medium consists of three different regions: i) the compressed low density gas immediately behind the irregularly shaped forward shock, ii) compressed gas of severely reshaped clouds deep behind the front, and iii) remnants of destroyed clouds that have penetrated into the innermost parts of the bubble. The gas density distribution in Fig. 5 illustrates these three zones. The first is presented by a dense ($n > 3 \text{ cm}^{-3}$) irregular shell. The next area adjoining and behind the shell consists of partly fragmented and in some cases merged dense ($n > 10 \text{ cm}^{-3}$) radially elongated clouds. The third case is presented by low density ($n \lesssim 0.1 - 1 \text{ cm}^{-3}$) envelopes around the clouds that originate due to instabilities of their surface and episodic encounters of the shocks from multiple SNe, and by their remnants in the form of diluted fragments and filaments with density $n < 0.03 \text{ cm}^{-3}$.

The first region mostly consists of a gas locked initially in the diffuse interclump medium, and in those clumps that have been initially located closer to the central area of the bubble and have been completely destroyed by the current epoch. The other two represent the material of the clouds that have been recently encountered by the forward shock and which have partly survived such an impact. Dust

¹ The code is available at <https://bitbucket.org/pandante/pyfc/src/master/>

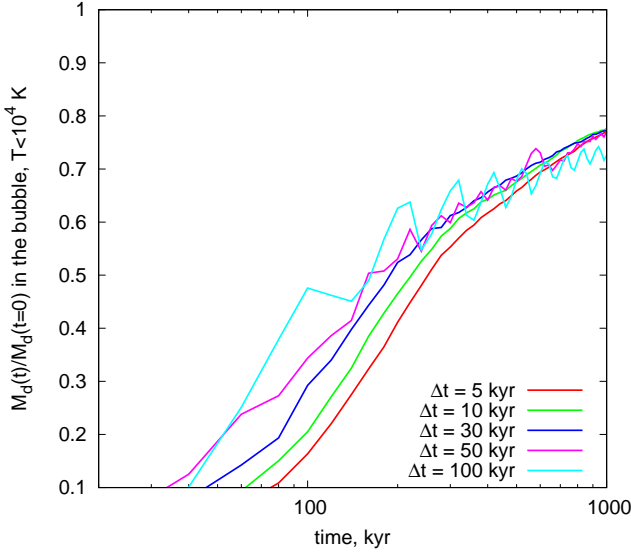


Figure 6. Mass fraction of the dust that can survive against sputtering, being locked *initially* (at $t = 0$) in dense clouds ($\rho > \langle \rho \rangle$) inside the region occupied by the bubble till the epoch t , i.e. the ratio of the mass of dust *remained in the clouds* at time t within the region outlined by the forward shock, $M_d(t)$, to the mass of dust locked in the clouds at $t = 0$, $M_d(t = 0)$. The bubble from multiple SNe explosions expands in a clumpy medium with an average density $\langle \rho \rangle = 1 m_H \text{ g cm}^{-3}$.

particles in these three regions experience different environmental influence, and in order to evaluate the fraction of surviving dust we have to approach them separately.

At early periods ($t \lesssim 200$ kyr), clumps located close to the innermost region are efficiently disintegrated with only a small part being swept up along with the expanding shell. The dust confined in such clouds is mostly destroyed. At later epochs, when the forward shock decelerates below 30–100 km s^{-1} ($\Delta t = 100$ and 5 kyr, respectively), the dense internal regions of the clouds survive along with the dust locked in them. A certain fraction of dust locked initially in clouds (the cloud dust) can leave their original reservoir and fill the hot intercloud medium, where the dust experiences strong sputtering. The cloud dust particles that remain in the low density and high temperature envelope of clouds are also expected to be destroyed.

In order to understand the overall picture of dust destruction within the region occupied by the remnant produced by multiple SNe in a cloudy medium, we illustrate in Fig. 6 how the dust locked initially (at $t = 0$) in the dense clouds is destroyed inside the region occupied by the bubble at redthe epoch t . More explicitly, this is the ratio of the mass of dust *that remain in the clouds* at time t within the region outlined by the forward shock, $M_d(t)$, to the mass of dust ($M_d(t = 0)$) locked in the clouds at $t = 0$. Note that $M_d(t)$ *does not account those dust particles that escaped* the original clouds and spread through the intercloud medium $\rho < \langle \rho \rangle$.

At early epochs $t < 100$ kyr, the fraction of surviving dust is very small because the dense cloud gas is strongly heated and disintegrated by the shock, as can be observed in Fig. 5. Correspondingly, dust associated with this gas does not survive much. At later times, clumps partly survive disruption from shock waves, resulting in the growth of the surviving dust mass. Before ~ 200 kyr the fraction is greater for higher SNe rate. However, this dependence becomes negligible at later epochs.

Another characteristic that describes the dust processing behind shocks is the mass *fraction of all dust* that survive against sputtering

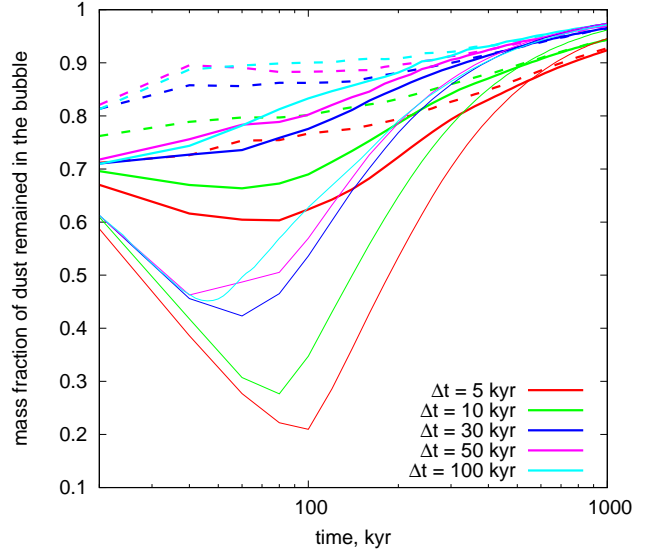


Figure 7. Mass fraction of the dust surviving against sputtering in a gas inside the *entire bubble outlined by the forward shock* driven by clustered SNe in a clumpy medium with the average density $\langle \rho \rangle = 1 m_H \text{ g cm}^{-3}$ (thick lines) and in a homogeneous medium with the same density (thin lines). Thick dashed lines depict the mass fraction of the dust inside clumps with density three times higher than the average value.

inside the *entire bubble outlined by the forward shock*. Fig. 7 presents this dependence by thick solid lines. At early times $t \sim 70$ kyr, this fraction decreases for the case of one SN per $\Delta t = 5$ kyr (red line). Later it begins to grow, thanks to dense lumps that survive in the bubble (Fig. 6). In a clumpy medium, a significant mass of dust contains in dense fragments, which are efficiently stripped only at early epochs. The mass fraction of the dust surviving against sputtering and associated with such dense clumps increases (see thick dashed lines in Fig. 7). Such gas includes dense lumps, compressed fragments and dense irregular shell. Later, the mass-loading of the flow behind the forward shock increases and the major part of the surviving dust remains associated with gas in dense clumps. This is shown by converging of thick dashed and solid lines in Fig. 7 at later times. For lower SN rate, the picture is qualitatively similar, however, more dust survives in the bubble because the destruction of dense fragments is less effective.

In the bubble expanding in a homogeneous medium, dust is efficiently destroyed by thermal and kinetic sputtering in the bubble's shell, while the the forward shock remains adiabatic. When the shock enters the radiative stage, dust particles decelerate in the dense cold layers due to drag force, and where they become protected against sputtering (Vasiliev & Shchekinov 2024).

When the bubble expands in a cloudy medium dust is destroyed (a) in completely destroyed clumps by the forward shock, (b) in the shell formed immediately behind the forward shock and (c) in the hot envelopes around lumps far behind the front due to stripping by shocks from continuous SNe explosions. The first two mechanisms play a role when the forward shock is quite strong and with the velocity higher than 200 km/s. In a clumpy medium the forward shock moves presumably in the interclump low-dense medium and maintains high velocity longer. Those parts of the shock that interact with the clumps and penetrate them with lower velocity and in which the dust locked in the denser clumps, remain protected against sputtering. Continuous SNe explosions result in multiple shocks so that high-velocity sound waves impinge on dense clumps that have sur-

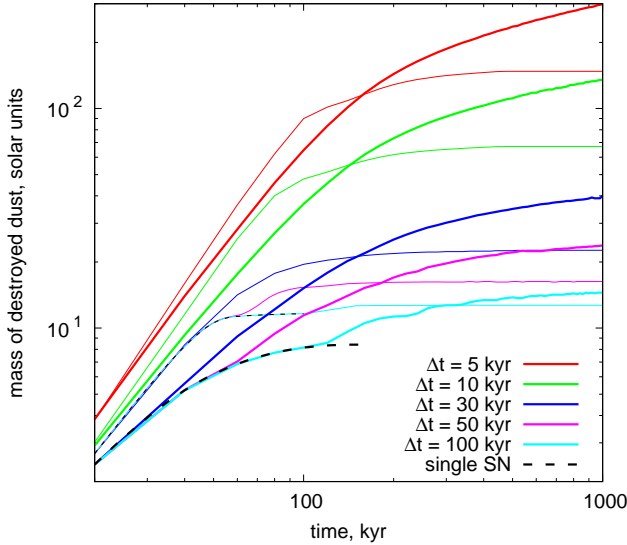


Figure 8. Mass of dust destroyed in the bubble evolved in a clumpy medium (thick lines) with mean density $\langle \rho \rangle = 1 \text{ cm}^{-3}$, the standard deviation $\sigma = 2.2$ for logarithmic value and maximum size of inhomogeneities equal to 16 pc. Thin lines depict the dust mass evolution in the bubble expanded in a homogeneous medium presented in Fig. 2.

vived the impact of the forward shock. These waves strip the clumps and form hot envelopes around them. Thus, deep behind the forward shock dust continues to income from destroyed gaseous fragments. As seen in Fig. 7, the first two processes (a) and (b) operate during about 300 kyr. The third one comes into play when all the remaining dust becomes locked in dense gas.

During the first several hundreds of kyr the fraction of surviving dust f_{surv} remains higher in the bubble expanding in a clumpy medium than in the one expanding in a homogeneous one (Fig. 7). Later on, f_{surv} in clumpy environment decreases because of continuous stripping of dense fragments (as seen in Fig. 7). Eventually at times $t > 100$ kyr the rate of surviving dust in a homogeneous medium becomes higher, because of the process (c) (of dust getting locked in dense clumps and destruction occurring only in the envelopes around them) becoming dominant at this phase, and at $t \gtrsim 300$ kyr the surviving fraction of dust in both cases turns to become of the same order.

Fig. 8 presents the mass of dust destroyed in the bubble for the same SN rates as shown in Fig. 2, but evolving in a clumpy medium. At early times, this mass (of destroyed dust) in the bubble evolving in a clumpy medium is lower than that in a homogeneous one. For SN rate $(\Delta t)^{-1} \sim (100 \text{ kyr})^{-1}$ the mass of dust destroyed during expansion in a clumpy medium begins to exceed the value reached in a homogeneous medium at an age of the bubble ~ 300 kyr. For higher SN rate this crossing occurs earlier, at ≈ 150 kyr, for all other rates.

We have earlier seen that in a homogeneous medium the mass of dust destroyed in the bubble becomes saturated after the shock speed falls below 200 km/s (see eq. 1). In a clumpy medium, dense fragments located deep behind the forward shock can supply dust into hot gas even after the forward shock decelerates below 200 km/s. Such fragments are stripped by shocks from ongoing SN explosions in the bubble. The characteristic time of this process depends on the density contrast roughly as $\propto \chi^{1/2}$. When outer layers of clumps stripped, the density contrast can reach $\gtrsim 10^2 - 10^3$ (Fig. 5). Further development of the Kelvin-Helmholtz instability becomes suppressed

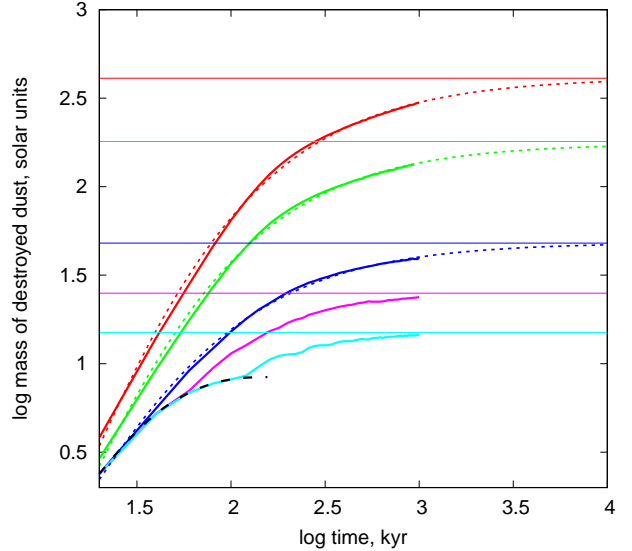


Figure 9. Mass of dust destroyed in the bubble evolved in a clumpy medium depicted in Fig. 8 (thick lines) and their fits (dotted lines, see the text for details). Thin lines show the saturation limits. The dashed line shows the mass of dust destroyed by a single SN.

and the destruction time for lumps of size ~ 10 pc (Fig. 5) exceeds tens of Myr (e.g. Klein et al. 1994; Poludnenko et al. 2002). Consequently, the dust mass destroyed in the bubble in a cloudy medium also saturates as in the homogeneous scenario, though at later ages. An increase in the SN rate leads to saturation at a later epoch. For instance, for the rate one SN per $\Delta t = 100$ kyr this has already reached till the age of ~ 800 kyr, and for $\Delta t = 50$ kyr this is expected to be at $\sim 1 - 1.5$ Myr. We anticipate similar behaviour for higher SN rate, which allows us to fit further evolution of the mass as $f(x) = a/[1 + \exp(-b(x - c))] - 0.5a$, where $x = \log(t, \text{kyr})$, $f(x) = \log(M_d, M_\odot)$, a , b , c are parameters. Fig. 9 presents the fits for three high values of SN rate. The fits come to saturation at ~ 10 Myr, which is several times longer than that in a homogeneous medium.

Accounting for the larger mass of dust destroyed in the bubble in a clumpy medium (Fig. 8), the dust destruction efficiency increases and becomes about 1.5–4 times higher in a clumpy medium compared to that in a homogeneous medium (compare red and grey lines in Fig. 10). The efficiency is increased for higher SN rate due to more frequent stripping events by impacts of clumps with high-velocity waves coming from SNe explosions. Smaller inhomogeneity in density (smaller value of density dispersion σ) leads to a decrease in this efficiency and shortening of the period for reaching saturation. For lower SNe rate the efficiency is expected to follow $\Delta t/t_{lf,max}$ similar to that in a homogeneous medium (Fig. 3).

4 DISCUSSION

It is well established that SN remnants are sources of IR emission (e.g. Dwek 1987; Graham et al. 1987; Arendt 1989; Meixner et al. 2006; Seok et al. 2013, 2015; Chawner et al. 2019, 2020). In young SN remnants such emission comes from dust produced by SN (Kozasa et al. 1989; Todini & Ferrara 2001; Nozawa et al. 2006). In older SN remnants the swept-up interstellar dust is expected to contribute mainly to this emission (e.g. Dedikov & Vasiliev 2025a). SN remnants are bright IR sources until dust remains dispersed in hot gas

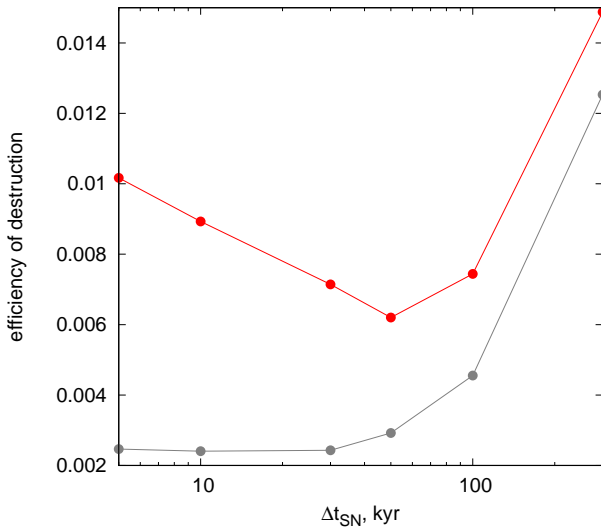


Figure 10. The dust destruction efficiency for the bubble evolved in a clumpy medium (red line) with mean density $\langle \rho \rangle = 1 \text{ cm}^{-3}$, the standard deviation $\sigma = 2.2$ for logarithmic value and maximum size of inhomogeneities equal to 16 pc. Grey line depicts the efficiency for the bubble evolved in a homogeneous medium as shown in Fig. 3.

inside the remnant. Dust grains located in hot gas can be destroyed by sputtering or move to gas in other thermal phases due to gas cooling or dynamical effects. Similar mechanisms occur in bubbles driven by multiple SNe explosions.

In the previous sections we explored the questions as to how interstellar grains are destroyed in SNe-driven bubbles and how destruction of the swept-up dust exhausts after the shell cools down. This dust passes rapidly across the hot layer and accumulates mostly in the cold shell, with a negligible amount left in the hot inner region. Thus, the swept-up dust does not contribute in the IR emission of the bubble after the dust stops to be destroyed in the bubble shell or at $t \gtrsim t_{sat}$ (eq. 1), when the shell velocity is of the order of $v_0 \sim 100 \text{ km s}^{-1}$.

Meanwhile, dust is injected in hot interior of the bubble by every subsequent SN explosion. The injected grains can become a significant source of IR emission as long as they survive in this hostile environment. The grain lifetime is roughly $\tau \sim 10^5 a_{\mu\text{m}} n_{\text{H}}^{-1} \text{ yr}$, and if this timescale is shorter than the time between subsequent SN explosions Δt_{SN} , then dust cannot accumulate in the hot interior. However, dust particles can leave the hot gas due to their high velocity, grains are caught up with the bubble shell and move in to colder gas, where they cannot emit efficiently.

In the bubbles evolving in a clumpy medium, the dust mass in hot gas is replenished by not only swept-up unprocessed interstellar dust, but also from stripped dense gaseous lumps far behind the forward shock of the bubble. Owing to the latter process, dust can be dispersed in the hot gas on longer timescales, exceeding several Myr, for SNe explosions more frequent than one SN per 30 kyr (see Fig. 9). Therefore, a bubble evolving in a clumpy medium can remain a bright IR source up to several Myr. Simultaneously, the hot plasma inside the bubble emits in X-ray. Due to continuous SNe explosions the plasma temperature is supported at $T_X \sim (2-4) \times 10^6 \text{ K}$ for SNe rate of one SN per $\sim 100-5$ kyr in bubbles older than several tens of kyr. Using the approach described in the paper (Dedikov & Vasiliev 2025a), we calculate the ratio between the IR and X-ray luminosities averaged over the whole bubble driven by multi-SNe. Usually the IR-to-X-ray ratio is used to determine the contribution of dust cooling

into radiative losses in hot plasma (Dwek 1987). We find that the ratio typically ranges between $\sim 1-30$. These values weakly depend on the SNe rate. However, a decrease of density contrast (density dispersion σ) in the ambient medium results in more efficient cloud destruction and, therefore, diminishing IR emission down to almost negligible values, for bubble older 100 kyr evolved in a homogeneous medium with $n \sim 1 \text{ cm}^{-3}$.

5 CONCLUSION

We have considered the destruction of dust in shells driven by multiple SNe explosions in stellar clusters. Using 3D hydrodynamic simulations, we have investigated how the single-size interstellar dust grains are destroyed in the multi-SNe bubble expanding in a homogeneous as well as clumpy medium. Our results can be summarized as follows:

- The mass of dust destroyed in the multi-SNe bubble does not grow after a certain epoch and becomes saturated, while SNe continue to explode. The timescale for this saturation is proportional to SNe rate in cluster;
- The mass of dust destroyed in bubble per SN decreases for higher SN rate; the destruction efficiency – the ratio of the the total mass of dust destroyed by clustered SNe to the value of dust destroyed by the same number of isolated SNe – in bubbles evolving in a homogeneous medium drops for higher mass clusters. E.g., around clusters with $M_* \gtrsim 4 \times 10^4 M_\odot$, it is less 0.4%. For lower mass clusters the efficiency is proportional to $\Delta t/t_{lf,max}$. Therefore, the destruction of the interstellar dust is controlled by SNe in low-mass clusters.
- The mass of dust destroyed by multiple SNe in clusters approximately 10% of that in an ensemble of equal number of isolated SN. Thus, the lifetime of dust in the ISM is longer by a factor ~ 10 compared to the value previously derived in the literature for isolated SN.
- In a clumpy medium the efficiency increases by about a factor of 1.5 in bubbles formed around clusters with $M_* \sim 4 \times 10^4 M_\odot$ and up to 4 times around $M_* \sim 8 \times 10^5 M_\odot$.

ACKNOWLEDGEMENTS

We thank Yuri A. Shchekinov for many valuable comments, Svyatoslav Dedikov for discussions.

DATA AVAILABILITY

The data underlying this article are available in the article.

APPENDIX A: RADIAL PROFILES

Figure A1 presents the angle-averaged radial profiles of gas density, temperature, dust density and sputtering timescale for a bubble formed by multiple SNe with time delay $\Delta t \sim 30$ kyr (upper panel). Due to their inertia, interstellar dust particles swept up together with gas by shock front move further into hot interior of the bubble (Vasiliev & Shchekinov 2024). There grains are subjected to sputtering. A supply of dust mass behind the front due to the bubble expansion is not sufficient to replenish its decrease by sputtering. This reveals in lower dust density in the shell at $t = 40$ kyr: the dust density (blue lines) does not follow the gas density (red lines). It is

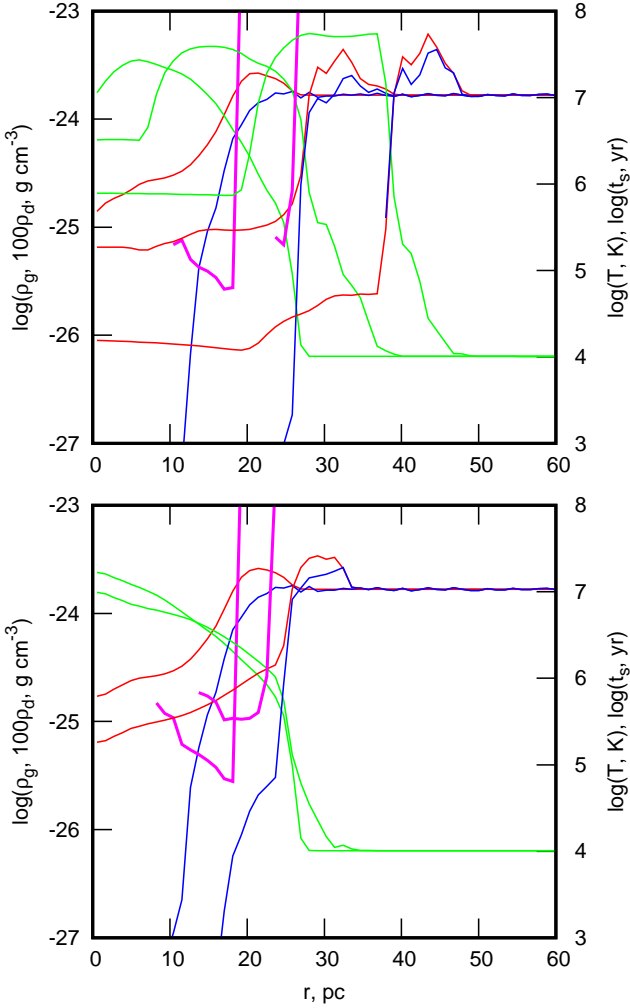


Figure A1. The angle-averaged radial profiles of gas density (ρ_g , red line), gas temperature (T_g , green line), density of the interstellar dust (ρ_d multiplied by a factor of 100, blue line) and sputtering timescale (magenta line) for the bubble formed by multiple SNe with rate $(\Delta t)^{-1} \sim (3 \times 10^4 \text{ yr})^{-1}$ (upper panel) at bubble age $t = 40, 100$ and 200 kyr (lines from left to right). The sputtering timescale at $t = 200$ kyr is longer than 10^9 yr. In lower panel the profiles are shown for a single SN of age $t = 40, 100$ kyr.

clearly seen that the dust density decreases by about a half order of magnitude at the maximum gas density compared to that expected for the absence dust destruction. If there had been no destruction of dust, then the densities of gas and dust would have followed each other (the red lines would coincide the blue ones).

When the shock velocity v_s falls below $v_s < 200 \text{ km s}^{-1}$, i.e. the temperature $T_s < 10^6 \text{ K}$, the sputtering becomes weaker $\rho_d/\dot{\rho}_d > t$, the delay between dust and gas profiles diminishes and the ratio ρ_d/ρ_g approaches a constant. Similar picture can be also found at the profiles for the bubble formed by a single SN explosion (lower panel).

REFERENCES

Arendt R. G., 1989, *ApJS*, 70, 181
 Barlow M. J., 1978, *MNRAS*, 183, 367

Bocchio M., Marassi S., Schneider R., Bianchi S., Limongi M., Chieffi A., 2016, *A&A*, 587, A157
 Borkowski K. J., Dwek E., 1995, *ApJ*, 454, 254
 Bychkov K. V., Pikelner S. B., 1975, *Soviet Astronomy Letters*, 1, 14
 Chawner H., Gomez H. L., Matsuura M., Smith M. W. L., Papageorgiou A., Rho J., Noriega-Crespo A., De Looze I., Barlow M. J., Cigan P., Dunne L., Marsh K., 2020, *MNRAS*, 493, 2706
 Chawner H., Marsh K., Matsuura M., Gomez H. L., Cigan P., De Looze I., Barlow M. J., Dunne L., Noriega-Crespo A., Rho J., 2019, *MNRAS*, 483, 70
 Dedikov S. Y., Vasiliev E. O., 2025a, *Astronomy Reports*, 69, 1
 Dedikov S. Y., Vasiliev E. O., 2025b, *New Astron.*, 114, 102293
 Draine B. T., 2009, in Henning T., Grün E., Steinacker J., eds, *Cosmic Dust - Near and Far* Vol. 414 of *Astronomical Society of the Pacific Conference Series*, *Interstellar Dust Models and Evolutionary Implications*. p. 453
 Draine B. T., 2011, *Physics of the Interstellar and Intergalactic Medium*. Princeton University Press
 Draine B. T., Salpeter E. E., 1979a, *ApJ*, 231, 438
 Draine B. T., Salpeter E. E., 1979b, *ApJ*, 231, 77
 Dunne L., Gomez H. L., da Cunha E., Charlot S., Dye S., Eales S., Maddox S. J., Rowlands K., Smith D. J. B., Auld R., Baes M., Bonfield D. G., Bourne N., Buttiglione S., Cava A., Clements D. L., Coppin K. E. K., Cooray A., Dariush A., de Zotti G., Driver S., Fritz J., Geach J., Hopwood R., Ibar E., Ivison R. J., Jarvis M. J., Kelvin L., Pascale E., Pohlen M., Popescu C., Rigby E. E., Robotham A., Rodighiero G., Sansom A. E., Serjeant S., Temi P., Thompson M., Tuffs R., van der Werf P., Vlahakis C., 2011, *MNRAS*, 417, 1510
 Dwek E., 1987, *ApJ*, 322, 812
 Graham J. R., Evans A., Albinson J. S., Bode M. F., Meikle W. P. S., 1987, *ApJ*, 319, 126
 Guillet V., Jones A., Pineau Des Forets G., 2009, in Boulanger F., Joblin C., Jones A., Madden S., eds, *EAS Publications Series Vol. 35 of EAS Publications Series*, *Dust dynamics and processing in shocks*. pp 219–241
 Iben Jr. I., 2013, *Stellar Evolution Physics, Volume 2: Advanced Evolution of Single Stars*. Cambridge, UK: Cambridge University Press
 Jones A. P., Tielens A. G. G. M., 1994, in Tielens A. G. G. M., ed., *The Diffuse Interstellar Bands The formation of small grains in shocks in the ISM*. pp 79–83
 Jones A. P., Tielens A. G. G. M., Hollenbach D. J., 1996, *ApJ*, 469, 740
 Jones A. P., Tielens A. G. G. M., Hollenbach D. J., McKee C. F., 1994, *ApJ*, 433, 797
 Kirchschlager F., Mattsson L., Gent F. A., 2022, *MNRAS*, 509, 3218
 Kirchschlager F., Schmidt F. D., Barlow M. J., Fogerty E. L., Bevan A., Priestley F. D., 2019, *MNRAS*, 489, 4465
 Klein R. I., McKee C. F., Colella P., 1994, *ApJ*, 420, 213
 Klingenberg C., Schmidt W., Waagan K., 2007, *Journal of Computational Physics*, 227, 12
 Korolev V. V., Vasiliev E. O., Kovalenko I. G., Shchekinov Y. A., 2015, *Astronomy Reports*, 59, 690
 Kozasa T., Hasegawa H., Nomoto K., 1989, *ApJ*, 344, 325
 Krumholz M. R., McKee C. F., Bland-Hawthorn J., 2019, *ARA&A*, 57, 227
 Lewis G. M., Austin P. H., 2002, in 11th Conference on Atmospheric Radiation, American Meteorological Society Conference Series, eds. G. Smith, and J. Brodie, pp 1–4
 Martínez-González S., Wünsch R., Silich S., Tenorio-Tagle G., Palouš J., Ferrara A., 2019, *ApJ*, 887, 198
 Mattsson L., 2021, *Research Notes of the American Astronomical Society*, 5, 288
 McKee C., 1989, in Allamandola L. J., Tielens A. G. G. M., eds, *Interstellar Dust Vol. 135, Dust Destruction in the Interstellar Medium*. p. 431
 Meixner M., Gordon K. D., Indebetouw R., Hora J. L., Whitney B., Blum R., Reach W., Bernard J.-P., Meade M., Babler B., Engelbracht C. W., et al. 2006, *AJ*, 132, 2268
 Michałowski M. J., Watson D., Hjorth J., 2010, *ApJ*, 712, 942
 Mignone A., Flock M., Vaidya B., 2019, *ApJS*, 244, 38
 Moseley E. R., Teyssier R., Draine B. T., 2023, *MNRAS*, 518, 2825
 Nath B. B., Laskar T., Shull J. M., 2008, *ApJ*, 682, 1055
 Nozawa T., Kozasa T., Habe A., 2006, *ApJ*, 648, 435

Péroux C., De Cia A., Howk J. C., 2023, MNRAS, 522, 4852

Poludnenko A. Y., Frank A., Blackman E. G., 2002, ApJ, 576, 832

Priestley F. D., Chawner H., Barlow M. J., De Looze I., Gomez H. L., Mat-suura M., 2022, MNRAS, 516, 2314

Rowlands K., Gomez H. L., Dunne L., Aragón-Salamanca A., Dye S., Maddox S., da Cunha E., van der Werf P., 2014, MNRAS, 441, 1040

Scheffler T., Sartorio N. S., Kirchschlager F., De Looze I., Barlow M. J., Schmidt F. D., 2025, arXiv e-prints, p. arXiv:2512.05046

Seok J. Y., Koo B.-C., Hirashita H., 2015, ApJ, 807, 100

Seok J. Y., Koo B.-C., Onaka T., 2013, ApJ, 779, 134

Sharma P., Roy A., Nath B. B., Shchekinov Y., 2014, MNRAS, 443, 3463

Slavin J. D., Dwarka E., Jones A. P., 2015, ApJ, 803, 7

Slavin J. D., Jones A. P., Tielens A. G. G. M., 2004, ApJ, 614, 796

Slavin J. D., Smith R. K., Foster A., Winter H. D., Raymond J. C., Slane P. O., Yamaguchi H., 2017, ApJ, 846, 77

Todini P., Ferrara A., 2001, MNRAS, 325, 726

Toro E., 2009, Riemann Solvers and Numerical Methods for Fluid Dynamics: A Practical Introduction. Springer Berlin Heidelberg

Vasiliev E. O., 2011, MNRAS, 414, 3145

Vasiliev E. O., 2013, MNRAS, 431, 638

Vasiliev E. O., Nath B. B., Shchekinov Y., 2015, MNRAS, 446, 1703

Vasiliev E. O., Shchekinov Y. A., 2024, MNRAS, 527, 8755

Vasiliev E. O., Shchekinov Y. A., Nath B. B., 2017, MNRAS, 468, 2757

Wang Y., Bao B., Yang C., Zhang L., 2018, MNRAS, 478, 2948

Youdin A., Johansen A., 2007, ApJ, 662, 613